Orientation of the **g**-Tensor Axes of the Rieske Subunit in the Cytochrome bc_1 Complex†

Michael K. Bowman,*,‡,§ Edward A. Berry,|| Arthur G. Roberts,§ and David M. Kramer§

W. R. Wiley Environmental Molecular Sciences Laboratory, Pacific Northwest National Laboratory, P.O. Box 999, K8-98, Richland, Washington 99352-0999, Ernest Orlando Lawrence Berkeley National Laboratory, Mailstop 3-520, 1 Cyclotron Road, Berkeley, California 94720, Calvin Laboratory 5230, University of California, Berkeley, California 94720-5230, and Institute of Biological Chemistry, Washington State University, 289 Clark Hall, Pullman, Washington 99164-6340

Received April 18, 2003; Revised Manuscript Received October 29, 2003

ABSTRACT: The orientation of the **g**-tensors of the Rieske iron−sulfur protein subunit was determined in a single crystal of the bovine mitochondrial cytochrome bc_1 complex with stigmatellin in the Q_o quinol binding site. The **g**-tensor principal axes are skewed with respect to the Fe−Fe and S−S atom direction in the 2Fe2S cluster, which is allowed by the lack of rigorous symmetry of the cluster. The asymmetric unit in the crystal is the active dimer, and the **g**-tensor axes have slightly different orientations relative to the iron−sulfur cluster in the two halves of the dimer. The $g \sim 1.79$ axis makes an average angle of 30° with respect to the Fe−Fe direction and the $g \sim 2.024$ axis an average angle of 26° with respect to the S−S direction. This assignment of the **g**-tensor axis directions indicates that conformations of the Rieske protein are likely the same in the cytochrome bc_1 and b_6f complexes and that the extent of motion of the Rieske head domain during the catalytic cycle has been highly conserved during evolution of these distantly related complexes.

The cyt[1] bc_1 complex is an essential component in the mitochondrial respiratory chain, and the structurally analogous cyt b_6f complex of chloroplasts plays a similar role in oxygenic photosynthesis (*1*). The cyt bc_1 complex is a dimeric integral membrane complex composed of as few as three subunits in some prokaryotes and up to 11 subunits in eukaryotes such as in bovine mitochondria. There are four essential, redox-active, metal centers in the complex: a Rieske iron−sulfur complex (2Fe2S) in the Rieske ISP, two *b*-type hemes with different redox potentials in a single cyt *b* protein, and a *c*-type heme in the cyt c_1 protein. The function of bc_1 (and b_6f) complexes is to catalyze the transfer of electrons from quinol to cyt *c* (cyt *f*) coupled tightly to the vectorial translocation of protons across the membrane. This proton translocation makes a vital contribution to the establishment of the proton motive force that drives the synthesis of ATP.

Electron transfer through the cyt bc_1 and b_6f complexes likely occurs through the so-called "Q-cycle", first proposed by Mitchell (*2*), and later modified by several groups (*3*−*7*). In the cyt bc_1 complex, ubiquinol (UQH_2) is oxidized at the quinol oxidase (Q_o) site, at the interface between the cyt *b* protein and the "Rieske" iron−sulfur protein (ISP) (*5*, *8*). Electron transfer from UQH_2 is bifurcated so that the first electron is transferred to the 2Fe2S cluster, leaving an unstable semiquinone species at the Q_o site, which is oxidized by cyt b_L. The two protons from the quinol oxidized at the Q_o site are released to the p-side of the membrane (i.e., in the case of mitochondria, the intermembrane space). After two turnovers of the Q_o site, the two electrons sent to the low-potential chain reduce UQ at the Q_i site to UQH_2, with an uptake of two protons from the n-side of the membrane (i.e., the matrix). Overall, for each electron transferred to the 2Fe2S cluster, two protons are shuttled to the p-side of the membrane.

The bifurcated electron transfer has a high yield, in both cyt bc_1 [reviewed by Muller *et al.* (*9*), and references therein] and b_6f complexes (*10*), implying that short-circuiting side reactions which bypass bifurcation are minimized.

Because such bypass reactions are strongly favored by thermodynamics (*7*, *11*, *12*), a catalytic switch was proposed to gate electron transfer at the Q_o site and prevent side reactions (*8*, *13*−*15*). One such switch has been suggested by the recent series of bc_1 crystal structures of the mitochondrial bc_1 (*1*, *16*). Different crystal forms and crystals grown in the presence and absence of Q_o inhibitors show the hydrophilic "head" domain of the ISP in several different

† This work was supported by National Institute of General Medical Science Grant GM61904 (M.K.B.), by U.S. Department of Energy Grant DE-FG03-98ER20299 (D.M.K.), and by Grant R01DK44842 (E.A.B.). The W. R. Wiley Environmental Molecular Sciences Laboratory is a national scientific user facility sponsored by the Department of Energy's Office of Biological and Environmental Research and located at Pacific Northwest National Laboratory.

* To whom correspondence should be addressed. Phone: ++(509)-376-3299. Fax: ++(509)-376-2303. E-mail: Michael.bowman@pnl.gov.

‡ Pacific Northwest National Laboratory.

§ Washington State University.

|| Ernest Orlando Lawrence Berkeley National Laboratory and University of California.

[1] Abbreviations: CW, continuous wave; cyt, cytochrome; cyt b_6f, plastoquinol plastocyanin oxidoreductase; cyt bc_1, ubiquinol cytochrome *c* oxidoreductase; EFG, electric field gradient; ENDOR, electron nuclear double resonance; EPR, electron paramagnetic resonance; ESE, electron spin echo; ESEEM, ESE envelope modulation; ISP, iron−sulfur protein; NCS, noncrystallographic symmetry; Q_o, quinol oxidase; rms, root-mean-square; UQ, ubiquinone; UQH_2, ubiquinol; WT, wild-type; 2Fe2S, two-iron and two-sulfur.

10.1021/bi034620z CCC: $27.50
Published on Web 12/19/2003

positions. One position, termed ISP_B, places the ISP close to the distal niche of the Q_o site with ligands of the 2Fe2S cluster in contact with the Q_o site. The other position, termed ISP_C, places the ISP close to cyt c_1, while in some crystals, the ISP is located in intermediate positions. In the bovine mitochondrial bc_1 crystals, the ISP headgroup pivots by ~65°, moving the 2Fe2S cluster by 21.2 Å. This pivoting action provides a mechanism for the catalytic switch that prevents both electrons from the quinol from flowing through the high-potential chain (*8*). The 2Fe2S cluster in the ISP can undergo only one-electron redox reactions and would have to pivot to ISP_C to be close enough to transfer an electron to cyt c_1 and pivot back before it can accept the second electron.

There is evidence that the redox properties of the 2Fe2S cluster are coupled to the position of the ISP. Brugna *et al*. (*17*) found that changing the redox state of the cluster imposed a different equilibrium position for the ISP headgroup. In a complementary fashion, Darrouzet *et al*. (*18*) and Crofts *et al*. (*19*) proposed that the redox properties of the 2Fe2S cluster are modulated by the position of the ISP. Together, these data imply that the redox transitions of the 2Fe2S cluster and the conformation of the ISP are coupled in some way. One can imagine redox coupling occurring either by changing the environment around the cluster (e.g., by altering H-bonded ligands to the 2Fe2S cluster imidazole) or by mechanical deformation of the cluster. Such coupling guides the reaction of Q_o site reactive species, thus inhibiting side reactions (*19*).

The reduced ISP has an anisotropic **g**-tensor, meaning that its EPR spectrum depends in a well-understood fashion on its orientation relative to the magnetic field of the spectrometer. The orientation of the **g**-tensor axes relative to the plane of the membrane is readily determined in samples of oriented membranes, and such EPR measurements have clearly demonstrated that the ISP does pivot by up to 60° in different physiologically relevant states. Thus, one would like to know the orientation of the **g**-tensor axes to determine the conformational changes of the ISP in the membrane because the **g**-tensor axes ought to be tied closely to the molecular axes of the cluster. This would allow determination of conformations under conditions that cannot be attained in crystals.

Additional impetus for understanding the **g**-tensor comes from observations that the 2Fe2S EPR line shape changes, sometimes dramatically, with various occupants in the Q_o site. The high-field peak corresponding to g_x shifts in *Rhodobacter capsulatus* cyt bc_1 upon titration of substrate quinone and quinol, suggesting that two quinones may bind simultaneously at the Q_o pocket (*20*, *21*). This observation resulted in the so-called "double-occupancy" catalytic models and has been applied to all bc_1 complexes. However, other authors argue that only one quinone species is involved (*22*, *23*). To date, the origin of the *g*-factor shifts remains unclear, but given the strong correlations among ISP conformation, Q_o site occupancy, and EPR line shape (*19*), a more detailed relationship should be established. Defining the origins of the g_x-shifts would allow rigorous experimental testing of some of the catalytic models.

The ISP *g*-factors are also very relevant to an additional aspect of cyt bc_1 and b_6f structure and function. EPR measurements on several systems suggest that ISP pivoting is a general feature of cyt bc_1 and b_6f complexes from eukaryotes, prokaryotes, and archaea (*17*, *24*−*27*). Membrane fragments containing an active, intact cyt bc_1 or b_6f complex are readily oriented on Mylar sheets for EPR measurements. One could use the **g**-tensor orientation to determine the conformations and movement of the ISP in states not available in crystals such as the bc_1 Q_o site occupied by ubiquinone, or in site-directed mutants.

Unfortunately, there are two incompatible assignments of the **g**-tensor axes to the molecular axes of the 2Fe2S cluster. Bertrand *et al.* (*28*) made one assignment on the basis of theoretical ligand field considerations, while Gurbiel *et al*. (*29*) made an alternate assignment on the basis of experimental ENDOR data. Current crystal structures show that the 2Fe2S cluster and its ligands have only approximate "symmetry"; hence, the **g**-tensor axes may deviate significantly from the molecular axes of the cluster. Recent EPR measurements of the 2Fe2S cluster in the b_6f complex (*27*) show a noticeable difference between the orientation of its **g**-tensor axes and the molecular axes of the 2Fe2S cluster in bc_1 crystals, and it is unclear whether this reflects a real difference in structure or a skewing of the **g**-tensor and molecular axes in the respective species.

This is a preliminary report on the determination of the **g**-tensor orientation of the ISP of the bovine mitochondrial bc_1 complex with stigmatellin from single-crystal EPR measurements. The orientation is generally consistent with ligand field theory (*28*) but shows subtle effects of crystal packing interactions on the orientation and/or principal values of the **g**-tensor.

MATERIALS AND METHODS

Protein Crystal. Crystals of bovine mitochondrial bc_1 inhibited with stigmatellin were grown in the Berry lab for X-ray diffraction studies (PDB entry 1PP9; L.-S. Huang, D. Cobessi, and E. A. Berry, in press). The crystals were grown with stigmatellin present and were not treated with redox reagents. The EPR data (below) show that the ISP and cyt *c* were at least partially reduced, but both cyt *b* hemes were oxidized. Stigmatellin is generally thought to form the same complex in the Q_o site as the natural quinol substrate but is incapable of reacting (*1*). This crystal provides a good structural model of the ISP_B conformation and of the active complex, including the hydrogen bond between the substrate and the ISP.

A typical crystal approximately 0.4 mm × 0.2 mm × 0.2 mm in size, grown originally for diffraction measurements, was drawn into a 1.1 mm (outside diameter) quartz EPR capillary (Wilmad Glass, Buena, NJ) together with a small drop of the mother liquor. The long axis of the crystal, which coincides with the crystallographic *c*-axis, aligned itself along the axis of the capillary. The sample was frozen and stored on dry ice or in liquid nitrogen until measurements were taken at 10 K. The crystal belongs to space group $P2_12_12_1$ with the cyt bc_1 dimer as the asymmetric unit.

EPR. EPR measurements were made on a Bruker ESP380E pulsed EPR/ENDOR spectrometer with a 3 mm Split Ring resonator and Flexline goniometer and cryostat with an Oxford ITC-503 temperature controller. The microwave frequency was measured with an EIP 575B counter. The sample was rotated around the capillary axis perpendicular

to the applied magnetic field in 10° steps through 360°. ESE signals measured as function of magnetic field were used to record the EPR spectrum at each orientation. Initial attempts using CW EPR with a field modulation of 100 kHz revealed that the EPR line width showed considerable *g*-strain, with the line width increasing rapidly as the deviation from g_z increased. In EPR, the conventional first-derivative signal amplitude is inversely proportional to the square of the line width, so the EPR signal became undetectable for *g*-factors of <1.95. In the ESE spectrum, peak height is linearly proportional to the reciprocal of the line width, offering better relative sensitivity for broad lines. However, the ESE signal of the ISP has a periodic modulation of intensity known as ESEEM that is so severe at some orientations that it makes the ESE signal vanish. To avoid that, relatively broad microwave pulses of 120 and 240 ns were used to generate the echo. These long pulse widths allow use of lower microwave powers and higher resonator *Q* values while eliminating much of the ESEEM.

Data Analysis. The resonant fields and the effective *g*-factors of peaks in the EPR spectra were measured using the WIN-EPR software package from Bruker. The widths at half-height of the EPR lines were as much as 6 mT at some orientations, making it difficult to determine the precise peak position in the presence of significant noise. In those cases, a moderate amount of spectral smoothing was used to help locate the position of the peak. An examination of EPR line positions as a function of crystal orientation revealed three traces consistent with rotations of the known *g*-factors of the ISP and a few other peaks that could be either large-amplitude excursions of noise or EPR lines from oxidized hemes in cyt bc_1. In addition, there was a background signal from the resonator due to Cu(II) that forms on an exposed copper surface in the microwave coupling loop.

The line positions and corresponding microwave frequencies of EPR lines consistent with the ISP were then used as input to the computer program EPR-NMR (Department of Chemistry, University of Saskatchewan, Saskatoon, SK) which performed least-squares fits of spin Hamiltonian parameters to the input considering both the space group symmetry of the crystal and possible misalignment of the crystal. Structures were visualized and manipulated using Swiss PDB-Viewer version 3.7 and POV version 3.5. Additional calculations were performed using Mathematica version 4.2, and plots were generated with SigmaPlot 2001.

RESULTS

*The **g**-Tensor Is Different for the Two ISPs in the Asymmetric Unit.* The cyt bc_1 dimer is the asymmetric unit in this crystal, and there is one 2Fe2S cluster in the Rieske ISP of each monomer comprising the dimer. In the $P2_12_12_1$ space group, there are four symmetry-related sites for each monomer, but not all four sites can be distinguished in a magnetic resonance measurement (*30*). When the applied magnetic field is perpendicular to one of the crystal symmetry axes, there are degeneracies resulting in at most two distinct sites per monomer. The space group and the overall orientation of the bc_1 complex within the crystal are the same as in crystals of the chicken bc_1 complex (PDB entries 1BCC and 3BCC). Those chicken bc_1 complexes were analyzed in terms of a NCS element relating the two halves of the dimer. To the extent that the NCS generated identical monomers in the chicken dimer, the ISP in both monomers would have identical EPR parameters. Examination of the bovine crystal structure showed no obvious differences in the structure of the ISP headgroup between the two monomers that comprise the asymmetric unit.

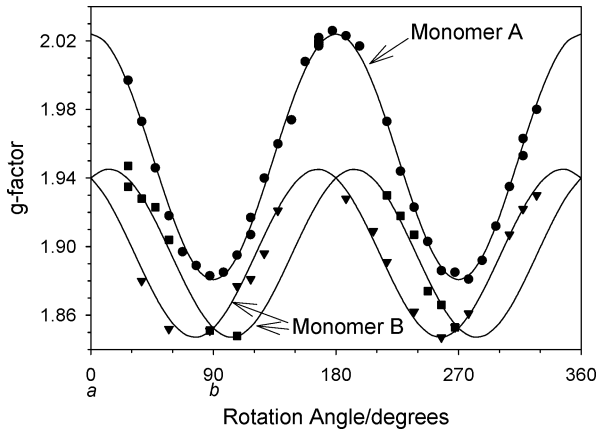

FIGURE 1: *g*-Factor of the Rieske ISP as a function of rotation about the crystal *c*-axis. The solid lines are the fits to the individual monomers in the asymmetric unit. Experimental data points: (●) monomer A and (■ and ▼) two distinct sets of symmetry-related sites in monomer B. The directions corresponding to the *a*- and *b*-axes are indicated below the rotation angles.

In view of this NCS element, the initial hypothesis was that the two monomers have identical **g**-tensors whose orientations are related by the NCS. This hypothesis results in considerable simplification in data acquisition and analysis. Single-crystal EPR measurements for the complete determination of a **g**-tensor normally require rotation of the magnetic field in three orthogonal planes. However, when the crystal contains several magnetically distinct, symmetry-related sites, the measurement of each of those sites during rotation in a single plane is equivalent to a rotation in a different plane for each of those sites, as described by Weil *et al.* (*30*). For the bovine bc_1 crystal, rotation about one of the 2-fold axes or the hypothesized NCS axis generates the same data as rotation in four different planes related by those symmetry elements. Thus, a single rotation about the *c*-axis of the crystal would generate sufficient data for the complete determination of the **g**-tensor and its orientation without the errors resulting from remounting the crystal. The quality of the fits to the experimental data provides a stringent test of this hypothesis.

An examination of the *g*-factors plotted as a function of the rotation angle (Figure 1) shows a set of data points falling along a sinusoidal path between a *g* of ∼2.03 and ∼1.88, a range of ∼23 mT. This set of data will be called monomer A for convenience and corresponds to one of the monomers in the bc_1 dimer. The g_z-axis happens to be coincident with the *a*-axis of the crystal so that the expected pair of tracks are coincident. The majority of the remaining points in the rotational pattern fall along a pair of sinusoidal tracks that do not cross the track from monomer A. Each track ranges between a *g* of ∼1.94 and 1.85 but shifted in phase with respect to each other and to monomer A. They are assigned to two sets of symmetry-related sites from the other monomer, B.

Table 1: **g**-Tensors and Direction Cosines for the Reduced ISP in a Crystal of Bovine Mitochondrial Cyt bc_1 with Stigmatellin

g-tensor	principal values	direction cosines
Monomer A (ISP Chain E)		
		Axes: *a* *b* *c*
$\begin{pmatrix} 2.0240 & 0.0000 & -0.0001 \\ 0.0000 & 1.8805 & 0.0293 \\ -0.0001 & 0.0293 & 1.7995 \end{pmatrix}$	$\begin{pmatrix} 2.024 \\ 1.89 \\ 1.79 \end{pmatrix}$	$\begin{pmatrix} 1.00000 & 0.00012 & 0.00026 \\ -0.00004 & 0.95121 & -0.30853 \\ -0.00028 & 0.38530 & 0.95121 \end{pmatrix}$
Monomer B (ISP Chain R)		
		Axes: *a* *b* *c*
$\begin{pmatrix} 1.9375 & -0.0232 & 0.0962 \\ -0.0232 & 1.8518 & 0.0449 \\ 0.0962 & 0.0449 & 1.9147 \end{pmatrix}$	$\begin{pmatrix} 2.024 \\ 1.89 \\ 1.79 \end{pmatrix}$	$\begin{pmatrix} 0.73226 & 0.46985 & 0.49300 \\ 0.07776 & -0.77685 & 0.062487 \\ 0.67658 & -0.41923 & -0.60538 \end{pmatrix}$

EPR-NMR was used to fit a **g**-tensor to the data from both monomers using rotation matrices describing the crystallographic symmetry and the hypothesized NCS. The NCS matrix relating the two monomers was constructed to superimpose the ISP headgroups in the crystal structure. The best fit of a **g**-tensor to the data using EPR-NMR did not yield a very good fit in a number of aspects. The fit has an rms deviation of 1.40 mT, which is significantly larger than the line width in many orientations. The principal values of the **g**-tensor had rather large error bars but did include the full range of values reported for bc_1 with stigmatellin. Also, there were systematic deviations between the best fit and the experimental data over a wide range of orientations. These aspects of the fit raise serious concern that the original hypothesis is invalid, and consequently, other fits to test that hypothesis were undertaken.

A series of fits were made allowing the two monomers to have different **g**-tensors, which presented a problem. There is only experimental rotational data in two independent planes for each monomer. The data are incomplete for the determination of the full **g**-tensor of either monomer. Additional measurements for obtaining a complete data set for each monomer did not appear to be practical for two reasons. (1) The *g*-strain is largest near the g_y-g_x plane needed for a complete data set, and the available X-band EPR spectrometer lacked adequate sensitivity for measurements in that plane. (2) The single-axis goniometer used for these measurements does not allow accurate remounting of the crystal and would produce unacceptable uncertainty in the data.

However, there is independent information that can be used to supplement the measurements presented here. The EPR spectrum of cyt bc_1 and b_6f inhibited with stigmatellin has been studied in a wide range of samples from intact cells and organelles through the isolated complex and has very consistent *g*-factors. Thus, the principal values of the **g**-tensor in the crystal are rather tightly constrained unless the crystal produces an unprecedented environment or conformation. With the inclusion of this prior information about the principal values, it is possible to achieve the original goal of establishing the orientation of the **g**-tensor axes relative to the molecular axes of the 2Fe2S cluster.

A series of fits were made using EPR-NMR in which the principal values of the **g**-tensor were fixed at the values (1.79, 1.89, and 2.024) reported for bovine cyt bc_1 with stigmatellin in solution (*31*), but with the orientations of the **g**-tensor allowed to vary independently for the two monomers. The best fit was quite good with an rms deviation of 0.67 mT and showed no systematic deviation from the experimental data (Figure 1). Subsequent fits with **g**-tensor principal values bracketing the range reported for cyt bc_1 with stigmatellin yielded the same rms deviation and **g**-tensor orientations that varied by at most 4°. Thus, over the entire range of *g*-values reported for the Rieske 2Fe2S cluster in cyt bc_1 with stigmatellin, the **g**-tensor orientation is nearly invariant.

The fit based on the hypothesis of identical **g**-tensors for the two monomers in the asymmetric unit is significantly worse ($p < 0.001$) than the fits with different tensors, and therefore, the original hypothesis must be rejected. On the basis of this inability to adequately fit the experimental data, it must be concluded that the two monomers in the asymmetric unit have **g**-tensors that differ in orientation and/or principal values. The results obtained with a single set of principal values (1.79, 1.89, and 2.024) (*31*) will be used in the rest of this paper because the primary focus is on determining the orientation of the **g**-tensor axes and because the orientations obtained from the fits are largely invariant over the range of reported *g*-values.

*The **g**-Tensor Orientation Matches Ligand Field Theory Predictions.* The fits to the experimental data determine the **g**-tensor for one of the symmetry-related sites in the crystal. That tensor must be assigned to a particular site to determine its orientation relative to the molecular structure. An assignment must be made for each ISP (labeled chains E and R in the crystal structure). Only one set of assignments met the strict criteria of consistency with the EPR of oriented membranes, consistency with the model of Bertrand *et al.* (*28*) and the data of Gurbiel *et al.* (*29*), and similar orientations in both monomers. The **g**-tensors in the crystal axis system are listed in Table 1.

A set of orthogonal molecular axes (*Fe*, *S*, and *p*) was defined for both ISP with one axis, *Fe*, along the Fe−Fe vector of the 2Fe2S cluster. Another axis, *p*, is perpendicular to the *Fe*-axis and the S−S vector, and the *S*-axis is perpendicular to both. The orientation of the **g**-tensor for both monomers is shown in Figure 2, and the direction cosine matrices and the angles between the **g**-tensor and molecular axes are given in Table 2. This assignment agrees with the EPR of oriented membranes of both bc_1 and b_6f which show that the g_y-axis, roughly perpendicular to the plane of the 2Fe2S cluster, lies in the plane of the membrane in the presence of stigmatellin (*17*, *24*−*27*). The axis assignment also agrees with that of Bertrand *et al.* based on ligand field considerations assuming perfect C_{2v} or D_2 symmetry for the cluster. It disagrees with the assignment of Gurbiel *et al.*

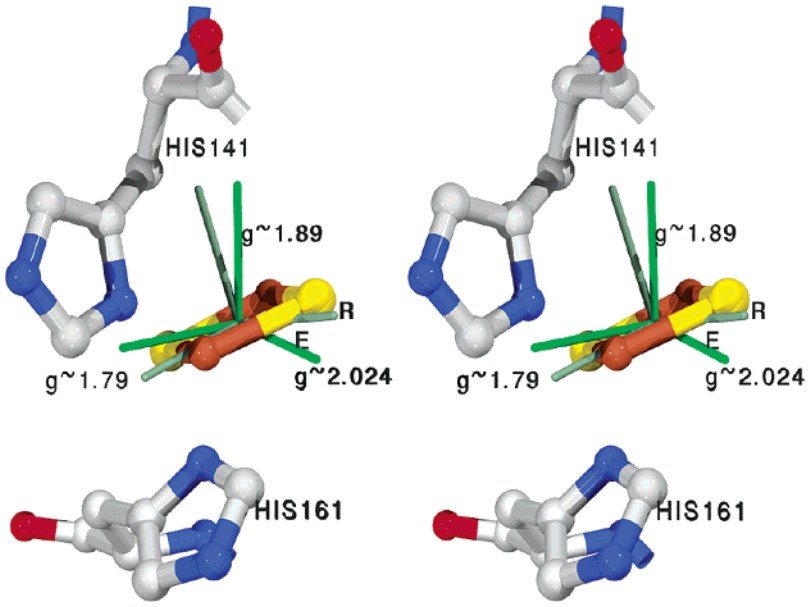

FIGURE 2: Orientation of the **g**-tensor axes of monomer B in chain R (gray) and monomer A in chain E (green) relative to the molecular axes of the cluster. The two histidine ligands to the cluster are shown to provide its orientation, but the two cysteine ligands on the other Fe are not. This figure is drawn for "wall-eyed" or defocused stereoviewing.

Table 2: Direction Cosines Relating the **g**-Tensor Axes to the Molecular Axes and Angles between the Axes for the Reduced ISP in a Crystal of Bovine Mitochondrial Cyt bc_1 with Stigmatellin

g-value	Direction Cosines *Fe*-axis	*S*-axis	*p*-axis
Monomer A (ISP Chain E)			
2.024	−0.49399	0.41200	0.76566
1.89	0.81420	−0.08974	0.57360
1.79	−0.30503	−0.90676	0.29112
Monomer B (ISP Chain R)			
2.024	−0.29138	0.17315	0.94081
1.89	0.95331	−0.02898	0.30059
1.79	−0.07932	−0.98447	0.15662

Angles between Axes	monomer A	monomer B
$Fe-g_x$	40°	20°
$S-g_z$	36°	18°
$p-g_y$	25°	10°

(*29*) which interchanged the directions of the $g \sim 1.79$ and $g \sim 2.024$ axes but for understandable reasons. Their assignment is based on experimental ENDOR data from the histidine nitrogens. The dipolar hyperfine interactions directed along the N−Fe bond indicated an N−Fe−N angle of either 80° or 100° depending on the axis assignment. Expecting that the Fe(II) ligand geometry would be nearly tetrahedral, they chose the value closer to the tetrahedral angle of ∼109°. The subsequent crystal structures show that the N−Fe−N angle is actually ∼91°, a value consistent with either assignment.

The **g**-tensor orientations are fairly close to each other even though the orientations and/or the principal values cannot be identical for the two monomers. The obvious *g*-strain in all EPR spectra of unoriented samples of cyt bc_1 makes it likely that the principal values in the crystal differ slightly. Some of the apparent difference in orientation seen in Figure 2 may arise in the fitting process from differences in principal values. However, the 15−20° differences in the orientation in Figure 2 are much larger than the 3−4° variation in the orientation seen in fits bracketing the range of observed principal values. A substantial portion of the difference in the orientation of the **g**-tensor in the two monomers of the asymmetric unit must be real.

In any case, the **g**-tensor axes do not coincide with the molecular axes. All attempts to fit the experimental data with a **g**-tensor coincident with the molecular axes failed, neither coming close to the data points nor returning reasonable **g**-tensor principal values. Thus, the **g**-tensor axes deviate significantly from the molecular axes of the 2Fe2S cluster in the ISP ($p < 0.001$).

DISCUSSION

The general direction of each principal **g**-tensor has important implications for the electronic structure of the 2Fe2S cluster and its role in electron transfer reactions. The **g**-tensor axes are oriented basically as proposed by Bertrand *et al.* (*28*) from ligand field considerations which confirm the basic model used for the cluster. However, Gurbiel *et al.* (*29*) point out that there is no self-consistent interpretation of **g**-tensor, ENDOR, and Mössbauer data, indicating "large gaps in our understanding of the electronic structures of the simplest 2Fe2S clusters". It was always tacitly assumed that the principal axes of all these magnetic interactions coincided with each other and with the molecular axes of the cluster. We find real deviations of the **g**-tensors from the molecular axes. The expectation that the **g**-tensor and molecular axes should be aligned is based ultimately on the symmetry constraint that a **g**-tensor and other magnetic axes must coincide with a rigorous 2-fold or higher axis or mirror plane normal passing through the 2Fe2S cluster. In the absence of any better structural information, previous studies assumed that the 2Fe2S cluster had orthorhombic symmetry, either C_{2v} or D_2, that would require exact alignment of magnetic

and molecular axes. The ISP lacks any symmetry, leading to the skewed axes for the **g**-tensor. The **g**-tensor, ^{57}Fe hyperfine interaction, and EFG can all have different axis systems, which is probably the reason that Gurbiel *et al*. found that a self-consistent interpretation based on coincident axes is impossible. The angles between the axes of the different quantities are important but often elusive experimental values that may be required to completely understand EFG, hyperfine, and *g*-factor data (*29*, *32*).

The difference in the orientation of the **g**-tensor axes in the 2Fe2S cluster of chain E versus chain R seems quite real. Its origin appears to lie in the *g*-strain that dominates the line width of Rieske and other 2Fe2S ISPs (*33*). The orientation of the **g**-tensor axes is sensitive to structural variations because there are no symmetry constraints on the principal axis directions of the **g**-tensor. Thus, the difference in orientation indicates that the two halves of the bc_1 dimer in the crystal adopt slightly different structures caused by different environments, different contacts, and different crystal packing forces in their respective crystal sites.

We looked closely for differences between the structures of the two monomers in the asymmetric unit even though they are nominally in the same ISP_B conformation. Little difference was observed in the structure of either the ISP or cyt *b*. The two monomers differ slightly at the ISP−cyt *b* interface, mainly in the angle of approach differing by 2.6°. Whether the approach angle and interactions at the ISP−cyt *b* interface or whether subtler structural differences are responsible for the observed skewing of the orientation of the **g**-tensors is hard to say.

Yet whatever alters the orientation of the **g**-tensor is likely also the source of the *g*-value changes allegedly caused by binding of substrate as hypothesized in the Q_o site double-occupancy model (*20*). The changes in *g*-values observed with different treatments of the cyt bc_1 complex probably have more to do with changes in the interactions at the ISP surface than with anything that happens in the Q_o binding pocket (*21*).

This paper emphasizes the intradimer differences in the orientations of the **g**-tensor axes. Yet it is important not to lose sight of the fact that the axes on each monomer do have very similar orientations that largely agree with the theoretical ligand field analysis (*28*), and that the discrepancies with the earlier ENDOR measurements (*29*) are now understood. There is a firm basis for applying this experimentally determined orientation to protein complexes with structurally homologous ISPs. The immediate surroundings of the 2Fe2S cluster are well-conserved in the soluble domains of the Rieske ISP in crystal structures of the bovine mitochondrial cyt bc_1 complex (*34*) and the spinach chloroplast cyt b_6f complex (*35*) and even in the 1.1 Å resolution structure of the Archaea *Sulfolobus acidocaldarius* (*36*). Thus, the overall orientation of the **g**-tensor should also be well-conserved. Yet the relatively large *g*-strain and the *g*-shifts observed for the ISP in different conformations make it important to extend these single-crystal EPR measurements to the ISP from other species, in other crystal forms and conformations. Such measurements will be made easier by the much greater sensitivity of high-frequency EPR spectrometers for diffraction-sized protein crystals and are planned for the future.

Oriented membranes containing cyt bc_1 and b_6f complexes (*17*, *25*, *27*) exhibit qualitatively identical behavior in the orientations of their respective ISP **g**-tensor axes. We have applied the **g**-tensor orientations found here to oriented membranes of b_6f (A. G. Roberts, M. K. Bowman, and D. M. Kramer, manuscript in preparation) and find a small difference in the orientation of the 2Fe2S cluster in the ISP_B conformation relative to cyt bc_1, but that the transition to the analogue of the ISP_C conformation involves the same rotation. This similarity implies that the conformations of the 2Fe2S cluster, as well as the degree of motion during each step of the catalytic cycle, have been highly conserved during the extended evolution of these functionally similar but distantly related enzyme complexes.

ACKNOWLEDGMENT

We thank John Weil and Michael Mombourquette for their help and guidance in the use of the EPR-NMR software.

REFERENCES

1. Berry, E. A., Guergova-Kuras, M., Huang, L. S., and Crofts, A. R. (2000) Structure and function of cytochrome *bc* complexes, *Annu. Rev. Biochem. 69*, 1005−1075.
2. Mitchell, P. (1975) The protonmotive Q cycle: A general formulation, *FEBS Lett. 59*, 137−139.
3. Crofts, A. R. (1985) The mechanism of the ubiquinol:cytochrome *c* oxidoreductases of mitochondria and of *Rhodopseudomonas sphaeroides*, in *The Enzymes of Biological Membranes* (Martonosi, A. N., Ed.) pp 347−382, Plenum Publishing Corp., New York.
4. Crofts, A. R., and Wang, Z. (1989) How rapid are the internal reactions of the ubiquinol: cytochrome *c2* oxidoreductase? *Photosynth. Res. 22*, 69−87.
5. Trumpower, B. L. (1990) The protonmotive Q cycle. Energy transduction by coupling of proton translocation to electron transfer by the cytochrome bc_1 complex, *J. Biol. Chem. 265*, 11409−11412.
6. Brandt, U., and Trumpower, B. (1994) The protonmotive Q cycle in mitochondria and bacteria, *Crit. Rev. Biochem. Mol. Biol. 29*, 165−197.
7. Brandt, U. (1996) Energy conservation by bifurcated electron transfer in the cytochrome bc_1 complex, *Biochim. Biophys. Acta 1275*, 41−46.
8. Zhang, Z., Huang, L., Shulmeister, V. M., Chi, Y. I., Kim, K. K., Hung, L. W., Crofts, A. R., Berry, E. A., and Kim, S. H. (1998) Electron transfer by domain movement in cytochrome bc_1, *Nature 392*, 677−684.
9. Muller, F., Crofts, A. R., and Kramer, D. M. (2002) Multiple Q-cycle bypass reactions at the Q_o site of the cytochrome bc_1 complex, *Biochemistry 41*, 7866−7874.
10. Sacksteder, C. A., Kanazawa, A., Jacoby, M. E., and Kramer, D. M. (2000) The proton to electron stoichiometry of steady-state photosynthesis in living plants: A proton-pumping Q cycle is continuously engaged, *Proc. Natl. Acad. Sci. U.S.A. 97*, 14283−14288.
11. Kramer, D., and Crofts, A. R. (1993) The concerted reduction of the high- and low-potential chains of the b_6f complex by plastoquinol, *Biochim. Biophys. Acta 1183*, 72−84.
12. Brandt, U. (1998) The chemistry and mechanics of ubihydroquinone oxidation at center P (Q_o) of the cytochrome bc_1 complex, *Biochim. Biophys. Acta 1365*, 261−268.
13. Baum, H., Silman, H. I., Rieske, H. S., and Lipton, S. H. (1967) On the composition and structural organization of complex 3 of the mitochondrial electron transfer chain, *J. Biol. Chem. 242*, 4876−4887.
14. Brandt, U., Haase, U., Schagger, H., and von Jagow, G. (1991) Significance of the "Rieske" iron−sulfur protein for formation and function of the ubiquinol-oxidation pocket of mitochondrial cytochrome *c* reductase (bc_1 complex), *J. Biol. Chem. 266*, 19958−19964.
15. Brandt, U. (1996) Bifurcated ubihydroquinone oxidation in the cytochrome bc_1 complex by proton-gated charge transfer, *FEBS Lett. 387*, 1−6.
16. Crofts, A. R., and Berry, E. A. (1998) Structure and function of the cytochrome bc_1 complex of mitochondria and photosynthetic bacteria, *Curr. Opin. Struct. Biol. 8*, 501−509.

17. Brugna, M., Rodgers, S., Schricker, A., Montoya, G., Kazmeier, M., Nitschke, W., and Sinning, I. (2000) A spectroscopic method for observing the domain movement of the Rieske iron−sulfur protein, *Proc. Natl. Acad. Sci. U.S.A. 97*, 2069−2074.
18. Darrouzet, E., Valkova-Valchanova, M., and Daldal, F. (2002) The [2Fe-2S] cluster E_m as an indicator of the iron−sulfur subunit position in the ubihydroquinone oxidation site of the cytochrome bc_1 complex, *J. Biol. Chem. 277*, 3464−3470.
19. Crofts, A. R., Shinkarev, V. P., Dikanov, S. A., Samoilova, R. I., and Kolling, D. (2002) Interactions of quinone with the iron−sulfur protein of the bc_1 complex: is the mechanism spring-loaded? *Biochim. Biophys. Acta 1555*, 48−53.
20. Ding, H., Robertson, D. E., Daldal, F., and Dutton, P. L. (1992) Cytochrome bc_1 complex [2Fe-2S] cluster and its interaction with ubiquinone and ubihydroquinone at the Q_o site: a double-occupancy Q_o site model, *Biochemistry 31*, 3144−3158.
21. Ding, H., Moser, C. C., Robertson, D. E., Tokito, M. K., Daldal, F., and Dutton, P. L. (1995) Ubiquinone pair in the Q_o site central to the primary energy conversion reactions of cytochrome bc_1 complex, *Biochemistry 34*, 15979−15996.
22. Snyder, C. H., Gutierrez-Cirlos, E. B., and Trumpower, B. L. (2000) Evidence for a concerted mechanism of ubiquinol oxidation by the cytochrome bc_1 complex, *J. Biol. Chem. 275*, 13535−13541.
23. Yu, C. A., Zhang, L., Deng, K. P., Tian, H., Xia, D., Kim, H., Deisenhofer, J., and Yu, L. (1999) Structure and reaction mechanisms of multifunctional mitochondrial cytochrome bc_1 complex, *Biofactors 9*, 103−109.
24. Brugna, M., Albouy, D., and Nitschke, W. (1998) Diversity of cytochrome *bc* complexes: example of the Rieske protein in green sulfur bacteria, *J. Bacteriol. 180*, 3719−3723.
25. Schoepp, B., Brugna, M., Riedel, A., Nitschke, W., and Kramer, D. M. (1999) The Q_o-site inhibitor DBMIB favours the proximal position of the chloroplast Rieske protein and induces a p*K*-shift of the redox-linked proton, *FEBS Lett. 450*, 245−250.
26. Brugna, M., Nitschke, W., Asso, M., Guigliarelli, B., Lemesle-Meunier, D., and Schmidt, C. (1999) Redox components of cytochrome *bc*-type enzymes in acidophilic prokaryotes. II. The Rieske protein of phylogenetically distant acidophilic organisms, *J. Biol. Chem. 274*, 16766−16772.
27. Roberts, A. G., Bowman, M. K., and Kramer, D. M. (2002) Certain metal ions are inhibitors of cytochrome b_6f complex 'Rieske' iron−sulfur protein domain movements, *Biochemistry 41*, 4070−4079.
28. Bertrand, P., Guigliarelli, B., Gayda, J.-P., Beardwood, P., and Gibson, J. F. (1985) A ligand-field model to describe a new class of 2Fe-2S clusters in proteins and their synthetic analogues, *Biochim. Biophys. Acta 831*, 261−266.
29. Gurbiel, R. J., Doan, P. E., Gassner, G. T., Macke, T. J., Case, D. A., Ohnishi, T., Fee, J. A., Ballou, D. P., and Hoffman, B. M. (1996) Active site structure of Rieske-type proteins: electron nuclear double resonance studies of isotopically labeled phthalate dioxygenase from *Pseudomonas cepacia* and Rieske protein from *Rhodobacter capsulatus* and molecular modeling studies of a Rieske center, *Biochemistry 35*, 7834−7845.
30. Weil, J. A., Buch, T., and Clapp, J. E. (1973) Crystal point group symmetry and microscopic tensor properties in magnetic resonance spectroscopy, *Adv. Magn. Reson. 6*, 183−257.
31. Ohnishi, T., Brandt, U., and von Jagow, G. (1988) Studies on the effect of stigmatellin derivatives on cytochrome *b* and the Rieske iron−sulfur cluster of cytochrome *c* reductase from bovine heart mitochondria, *Eur. J. Biochem. 176*, 385−389.
32. Fee, J. A., Findling, K. L., Yoshida, T., Hille, R., Tarr, G. E., Hearshen, D. O., Dunham, W. R., Day, E. P., Kent, T. A., and Münck, E. (1984) Purification and characterization of the Rieske iron sulfur protein from *Thermus thermophilus*: Evidence for a 2 Iron 2 Sulfur cluster having noncysteine ligands, *J. Biol. Chem. 259*, 124−133.
33. Hearshen, D. O., Hagen, W. R., Sands, R. H., Grande, H. J., Crespi, H. L., Gunsalus, I. C., and Dunham, W. R. (1986) An analysis of g-strain in the electron-paramagnetic-resonance of 2 [2Fe-2S] ferredoxins: evidence for a protein rigidity model, *J. Magn. Reson. 69*, 440−459.
34. Iwata, S., Saynovits, M., Link, T. A., and Michel, H. (1996) Structure of a water soluble fragment of the 'Rieske' iron−sulfur protein of the bovine heart mitochondrial cytochrome bc_1 complex determined by MAD phasing at 1.5 Å resolution, *Structure 4*, 567−579.
35. Carrell, C. J., Zhang, H., Cramer, W. A., and Smith, J. L. (1997) Biological identity and diversity in photosynthesis and respiration: structure of the lumen-side domain of the chloroplast Rieske protein, *Structure 5*, 1613−1625.
36. Bonisch, H., Schmidt, C. L., Schafer, G., and Ladenstein, R. (2002) The structure of the soluble domain of an archaeal Rieske iron−sulfur protein at 1.1 Å resolution, *J. Mol. Biol. 319*, 791−805.

BI034620Z